Biomaterials Science

ROYAL SOCIETY OF CHEMISTRY

PAPER

View Article Online
View Journal | View Issue

Cite this: *Biomater. Sci.*, 2025, **13**, 5122

Assessing the impact of CAP-p15 functionalization on the bioactivity of rough TiO_2-coated 316L stainless steel surfaces

Guadalupe Ureiro-Cueto, [a] Sandra E. Rodil, [b] José Ocotlán Flores-Flores,[c] Lía Hoz-Rodríguez, [a] Higinio Arzate †[a] and Gonzalo Montoya-Ayala *[a]

Stainless steel 316L (316L SS) is frequently used in implants and medical devices because of its low cost, high mechanical strength, and adequate biocompatibility. However, its bioinert nature limits osseointegration, often confining its applications to temporary uses. To address this issue, surface modifications such as oxide coatings and peptide adsorption have emerged as promising strategies to enhance the bioactivity of 316L SS. This study explores the surface modification of 316L SS substrates through sandblasting, followed by the deposition of a TiO_2 layer and subsequent biofunctionalization with a cementum attachment protein-derived peptide (CAP-p15) *via* physisorption using three different concentrations. The modified surfaces were characterized using X-ray photoelectron spectroscopy (XPS), scanning electron microscopy coupled with energy-dispersive X-ray spectroscopy (SEM/EDX), surface roughness analysis, and water contact angle measurements (WCA). Samples were incubated in artificial saliva (AS) for 21 days. The resulting peptide release, surface microstructure, the morphology and chemical composition of the deposits were evaluated. Additionally, human periodontal ligament cells (hPDLCs) were cultured on the modified surfaces to assess cell viability and attachment. Characterization revealed significant changes in surface chemistry, roughness, and wettability following functionalization. *In vitro* testing in AS demonstrated the formation of carbonated apatite, indicative of enhanced bioactivity. Furthermore, hPDLCs cultured on functionalized surfaces exhibited enhanced viability, improved adhesion, and enhanced cell spreading. These results suggest that peptide-based functionalization with CAP-p15 is a promising strategy for enhancing the osseointegration potential of 316L SS, offering valuable prospects for bone tissue regeneration.

Received 25th February 2025,
Accepted 8th July 2025

DOI: 10.1039/d5bm00294j

rsc.li/biomaterials-science

Introduction

In the biomedical field, metals represent approximately 70% of implants and medical devices produced owing to their high fatigue resistance, inertness, acceptable biocompatibility, long-term wear, corrosion resistance, and, in certain cases, low-cost production.[1,2]

The most used metals for these purposes are titanium (Ti), cobalt–chromium (Co–Cr) alloys, and stainless steel (SS). Each metal offers unique advantages depending on the application. Titanium and its alloys are recognized for their excellent biocompatibility and resistance to corrosion, mainly due to the development of a titanium oxide (TiO_2) layer during the passivation process. Co–Cr alloys are extremely resistant to corrosion and wear, which makes them suitable for high-load devices such as knee and hip replacements, heart valves, and fixation plates.[3]

Due to its low cost, mechanical strength, ductility, and acceptable biocompatibility, stainless steel (SS), particularly austenitic grade like 316L, is widely used in medical devices such as stents, screws, heart valves, and surgical wires. Nonetheless, 316L SS has limitations regarding corrosion resistance and osseointegration, making it more suitable for temporary applications. The primary concern with SS in biomedical settings is its vulnerability to corrosion when exposed to bodily fluids such as saliva and plasma, which create a corrosive environment that degrades the protective oxide layer and leads to the release of potentially cytotoxic metal ions, including nickel. This can trigger inflammatory responses and compromise long-term implant stability.[4–6]

[a]*Laboratorio de Biología Periodontal y Tejidos Mineralizados, División de Estudios de Posgrado e Investigación Facultad de Odontología, Universidad Nacional Autónoma de México, Mexico City, Mexico. E-mail: gonzaloma@fo.odonto.unam.mx*
[b]*Instituto de Investigaciones en Materiales, Universidad Nacional Autónoma de México, Circuito exterior S/N, Ciudad Universitaria, 04510 Mexico City, Mexico*
[c]*Instituto de Ciencias Aplicadas y Tecnología, Universidad Nacional Autónoma de México, Circuito Exterior S/N, Ciudad Universitaria, 04510 Mexico City, Mexico*
† Higinio Arzate is a senior author.

Given the critical role of bone–implant contact in achieving successful osseointegration, various surface modification techniques have been developed to enhance corrosion resistance and promote biological responses.[7] In this regard, surface modifications, such as roughness induced by mechanical abrasion (*e.g.*, sandblasting or acid etching) or the addition of bioactive materials like oxides and peptides, have been shown to improve cell attachment and osseointegration.[8,9]

Although the ideal surface roughness for enhancing osseointegration remains uncertain, surfaces with moderate roughness (Ra ~1–2 μm) are believed to elicit the most robust bone response.[10] Furthermore, incorporating titanium oxide layers on implants further enhances protein adsorption and promotes osteoblast interaction, improving overall bioactivity and implant performance.[11–13]

Recently, the use of short peptide sequences has emerged as a versatile method for enhancing implant surfaces, thanks to their straightforward synthesis methods, ability to improve cell behavior, and capability to facilitate mineral formation and osteogenic differentiation.[14–16]

Typically, these peptides are derived from extracellular matrix proteins such as fibronectin (FN) or bone sialoprotein (BSP). Nevertheless, the use of peptides derived from dental tissues for surface modification is still relatively unexplored. Studies have reported that proteins from dental tissues, such as Copine-7 (CPNE7), full-length amelogenin (AMELX), and extracts from dentin matrix acidic protein 1 (DMP1), can induce mineralization in mesenchymal stem cells.[17–20]

Cementum is a mineralized connective tissue which covers the roots of dental organs and provides anchorage for the collagen fiber bundles of the periodontal ligament and the supra-alveolar gingival fiber system, contributing to the biomechanical and structural support for the connective tissue attachment. Recently, a short peptide derived from the cementum attachment protein (HACD1/CAP; Accession: NM_AY455942.1; GI: 38503519), composed for 15 amino acids (here after named CAP-p15), has been shown to support the formation of carbonate hydroxyapatite crystals on amorphous TiO_2 surfaces, while also enhancing the proliferation and migration of human periodontal ligament cells (hPDLC) *in vitro*.[21]

Our previous work has demonstrated that CAP-p15 possesses a hydrophobic and acidic nature, which induces the mineral precipitation and promotes osteogenic differentiation when is used to functionalize TiO_2-coated substrates.[13] In these studies, atomically flat silicon (Si) substrates were utilized to isolate the effects of peptide functionalization, thereby minimizing the influence of surface roughness on the biological response.

This work reports on the use of rough 316L stainless steel (SS) surfaces coated with TiO_2 and biofunctionalized with CAP-p15, evaluating their physicochemical properties and potential to promote mineral formation while modulating cellular behavior. Our findings suggest that this bioactive surface enhances the biological performance of 316L SS, providing a promising strategy for improving bone tissue regeneration.

Experimental

CAP-p15 synthesis

The peptide synthesis was performed as described in the literature.[13] The peptide CAP-p15 was synthesized by the Fmoc (9-fluorenylmethyloxycarbonyl) solid-phase method and purified with C-18 reverse-phase liquid chromatography to achieve a purity level greater than 95% (Byosinth, Gardner, MA, USA). The lyophilized peptide was dissolved in distilled deionized water, filtered through a 0.22 μm filter, and stored at 4 °C before use.

Preparation of the substrates and TiO_2 coating deposition

316L stainless steel (316L SS) plates were cut into 1 cm^2 squares. Surface roughness was induced using a sandblasting method with SiO_2 particles, as previously described.[22,23] Before TiO_2 deposition, the plates underwent ultrasonic cleaning in acetone, followed by 2-isopropanol and dH_2O for 20 minutes each, then dried in a vacuum desiccator for 2 hours at room temperature (RT). The TiO_2 coating was applied *via* magnetron sputtering, following the protocol as described elsewhere.[24,25] Briefly, a high-purity titanium target (4-inch diameter) was used under deposition conditions of 20 mTorr pressure, with a mixed atmosphere of argon and oxygen (8/4.6 standard cubic centimeters per minute) as sputtering gases. We used for this magnetron sputtering a 200 W radio frequency power source.

316L SS/TiO_2 surfaces functionalization

Before functionalization, the surfaces were cleaned to remove any contamination. The 316L SS/TiO_2 surfaces were ultrasonically cleaned as previously described, dried in a vacuum desiccator for 1 hour, and sterilized under UV light before use. For the physical adsorption of CAP-p15 onto the 316L SS/TiO_2 surfaces, lyophilized CAP-p15 was dissolved in deionized water to final concentrations of 0.5 μg mL^{-1}, 1 μg mL^{-1}, and 1.5 μg mL^{-1}. The 316L SS/TiO_2 surfaces were coated with CAP-p15 solutions overnight. After incubation, the surfaces were dried and stored at RT. Bare 316L SS/TiO_2 surfaces were used as a control group.

Characterization studies

Morphology and elemental composition of 316L SS/TiO_2 substrates. To confirm the deposition of the TiO_2 layer, samples were analyzed using field emission scanning electron microscopy (FE-SEM, JSM-7800) equipped with energy-dispersive X-ray spectroscopy (EDX) for subsequent elemental analysis.

X-ray photoelectron spectroscopy analysis (XPS). The surface composition was analyzed using X-ray photoelectron spectroscopy (XPS) with a Physical Electronics Versa Probe II system, equipped with a scanning XPS microprobe. The measurements were conducted under an ultra-high vacuum condition of 4×10^{-8} Pa, with an energy source of Al Kα = 1486.6 eV. No argon pre-cleaning was performed to preserve the attached peptides. Charge compensation was done using a

dual ion-electron beam. The high-resolution spectrum was acquired using a pass energy of 20 eV with 0.1 eV resolution, and eight scans to accumulate enough signal. The data were analyzed using Multipack© version 9.9.3 software.

Roughness. Three random zones from each group were chosen to evaluate the topographic characteristics of pristine and treated substrates using a Zygo Nexview™ optical profilometer (Zygo Corporation, Middlefield, CT, USA). The average roughness (Sa) was obtained using the Mx™ software (version 6.4.0.21, Zygo Corporation, Middlefield, CT, USA).

Water contact angle (WCA) measurement. Contact angle measurement of functionalized and non-treated 316L SS/TiO_2 samples was evaluated through the sessile drop method using a goniometer OCA 15EC (DataPhysics Instruments, Filderstadt, Germany). Each sample analyzed received 4 μL of deionized water, and three sites were randomly selected to obtain an average of the contact angle. Images obtained were analyzed with SCA 20 software.

***In vitro* mineralization assay.** To evaluate the bioactivity of the samples both pristine and treated samples were immersed in an artificial saliva (AS) solution, as described in previous studies.[26–28] Each sample was placed in 10 mL of AS solution for 21 days at 37° C and a pH of 7.4, with the solution being refreshed every 3 days. After the incubation period, the samples were carefully removed, rinsed with deionized water, and dried at RT for further characterization.

Long-term stability assessment. To evaluate the long-term stability on the substrates, CAP-p15 peptide was labeled with Alexa Fluor 546 (AF-546) (Invitrogen) as described elsewhere.[21] Briefly, 5 μL of AF-546 in dimethylformamide solution (10 μg μL^{-1}) was added to 200 μL of peptide in PBS solution plus 20 μL of 1 M sodium bicarbonate. The solution was incubated for 1 h at RT. The non-labeled peptide was removed by dialysis with 4 changes every 4 h using 2 L of Tris buffered saline (TBS) solution, pH 7.4 with 1.0 kDa dialysis tubing (Spectrum Laboratories Inc., Rancho Dominguez, CA, USA). After freeze-drying, the samples were stored at 20 °C. The lyophilized labeled peptide was dissolved in deionized water to final concentrations of 0.5 μg mL^{-1}, 1 μg mL^{-1}, and 1.5 μg mL^{-1} and spread on 316L SS/TiO_2 surfaces and incubated for 1 h at RT. Subsequently, all coated 316L SS/TiO_2 surfaces (n = 3) were placed into 24-well plates and incubated in 750 μL of AS at 37 °C. The medium was collected and replaced after 24, 48, 72 h, and every 3 days thereafter until day 21, and the wells were supplemented with fresh AS. Fluorescence was measured with an ELISA plate reader (FilterMaxF5) at an excitation wavelength of 556 nm, with a wavelength correction set at 573 nm.

The concentration was calculated using a standard curve formula, and the cumulative release (%) of CAP-p15 was determined using the following equation:

$$d_r\% = \frac{m_x}{m_t} \times 100$$

where: d_r% is the percentage of cumulative CAP-p15 released at each time point, m_x is the mass of CAP-p15 released at each time point, and m_t is the cumulative CAP-p15 release in 21 days.

Scanning electron microscopy and energy-dispersive X-ray spectroscopy analysis (SEM/EDX). Before SEM analysis, the samples were coated with a thin layer of gold using vacuum-controlled sputtering equipment and mounted on metallic stubs with double-sided carbon tape. The distribution and morphology of calcium phosphate (CaP) deposits, as well as the Ca/P ratio, were assessed using field emission scanning electron microscopy (FE-SEM, JSM-7800) equipped with energy-dispersive X-ray spectroscopy (EDX).

ATR-FTIR analysis. Functional groups on pristine and functionalized surfaces were evaluated using ATR-FTIR in the range of 4000–500 cm^{-1} with a Nicolet FTIR model iS50R coupled to Smart iTX diamond-tipped equipment.

Cell culture. All experiments were performed in accordance with the Guidelines of the Declaration of Helsinki, and Experiments were approved by the ethics committee at the Faculty of Dentistry of the Universidad Nacional Autónoma de México (UNAM). Informed consents were obtained from human participants of this study. The Ethics Committee reviewed and approved the use of human tissue from the oral cavity for the generation and culturing of human periodontal ligament cells (hPDLC). The experimental studies used cells between the 2nd and 5th passages. The cells were grown and maintained in DMEM supplemented with 10% fetal bovine serum (FBS); (Thermo Fisher Scientific, Waltham, MA, USA), along with antibiotics (penicillin 100 UI mL^{-1}; streptomycin 100 μg mL^{-1}) in a 5% CO_2 and 95% air atmosphere.

Cell viability. Human periodontal ligament cells (hPDLCs) were cultured in DMEM supplemented with 10% fetal bovine serum (FBS); (Thermo Fisher Scientific, Waltham, MA, USA), along with antibiotics under standard conditions of 5% CO_2 and 37° C. Cells were plated at a density of 1×10^4 cells on surfaces treated with the three concentrations of CAP-p15 per well. Cell viability was analyzed after 24, 48 and 72 h with an MTT assay (3-(4,5-dimethylthazol-2-yl)-2,5-diphenyl tetrazolium bromide (Boehringer Mannheim, Indianapolis, IN, USA). Viability test was carried out incubating 300 μL of MTT solution (5 mg mL^{-1}) in PBS on each well for 4 h at 37° C. Subsequently, 100 μL of dimethyl sulfoxide (DMSO) was added to dissolve the formazan crystals. 100 μL were then taken and placed in 96-well plate (Nest Biotechnology Co) and absorbance was measured at 570 nm using a microplate reader FilterMax F5: Molecular Devices, Sunnyvale, CA, USA). Percentage of cell viability was calculated using the following equation:

$$\text{Cell viability}\,[\%] = \frac{\text{Absorbance of sample} - \text{absorbance of blank}}{\text{Absorbance of control} - \text{absorbance of blank}} \times 100$$

The absorbance value of control (hPDLCs cultured on polystyrene wells without CAP-p15) was normalized as 100% of cell viability.

Cell attachment assay. Human periodontal ligament cells (hPDLCs) were plated with a density of 2×10^3 over five different groups. The hPDLCs were plated over pristine surfaces (negative control), 316L SS/TiO_2 functionalized with fibronectin 5 μg mL^{-1} (used as a positive control to determine

100% of cell attachment) and 316L SS/TiO_2 treated with 0.5, 1, and 1.5 μg mL^{-1} of CAP-p15 (experimental samples). These groups were cultured for 24 h in DMEM- serum-free medium. Next, the medium was removed, and samples were washed with warm PBS (3×) to remove unattached cells. To quantify the percentage of attached cells we performed crystal violet staining according to Hayman.[29] Experiments were performed in triplicate and repeated twice.

To assess cell morphology, hPDLCs were fixed using sodium cacodylate buffer (0.1 M) and glutaraldehyde (2%), followed by washing with an ethanol gradient (20–100%). The surfaces then underwent a critical point process, were dried, and coated with gold. The images obtained from SEM were analyzed with ImageJ software (National Institutes of Health (NIH), Bethesda, MD, USA).

Statistical analysis

Results are expressed as Standard Error of the Mean (±SEM). An analysis of variance (ANOVA) was conducted to assess overall differences between groups, followed by Tukey's *post hoc* test to identify differences between data sets. The analysis was performed using GraphPad Prism 8 software (San Diego, CA, USA).

Results

Substrates morphology and elemental composition

Fig. 1 illustrates the surface characteristics of 316L SS substrates following TiO_2 deposition. SEM images revealed rough grooves and craters extending several microns on the substrates due to the sandblasting treatment. Mapping revealed the presence of elements such as Fe, Cr, Ni, O, and Ti.

X-ray photoelectron spectroscopy analysis (XPS)

The XPS survey (low-resolution spectra) are shown in Fig. 2a, containing the pristine 316L SS/TiO_2 surface and the samples after functionalization using the CAP-p15 peptide at the three concentrations. The spectrum of the pristine sample reveals the presence of C, O, Ti; no signal from the underlying stainless-steel substrate was detected for any sample (the position of the Fe 2p most intense signal is indicated in Fig. 2a for reference). Carbon concentration is due to the adsorption of carbonaceous species since the samples were exposed to the atmosphere, and no argon etching was used. Meanwhile, the O 1s signal is related to both oxygen bonded to Ti in the TiO_2 layer and to the adsorbed C. Therefore, detecting Nitrogen at very low concentrations provided by the peptide adsorption was fundamental to demonstrating the surface functionalization. It should be mentioned that measurements were performed at different zones of the 1 cm^2 samples. The sample with the lowest concentration (0.5 μg mL^{-1} of CAP-p15) showed a more uniform distribution, presenting the N 1s signal in all the tested areas, whereas the 1.0 and 1.5 μg mL^{-1} samples did not. Nevertheless, for the three functionalized samples, signal from N 1s was obtained. The high-resolution spectra were collected for all the elements in the samples. Still, only the N 1s are presented in Fig. 2b to show that the largest N content was detected for the 0.5 and 1.0 μg mL^{-1} samples, while the intensity decreased for the 1.5 μg mL^{-1} sample. This variation is reported in Fig. 2, where the atomic concentrations are reported for all samples, and it is

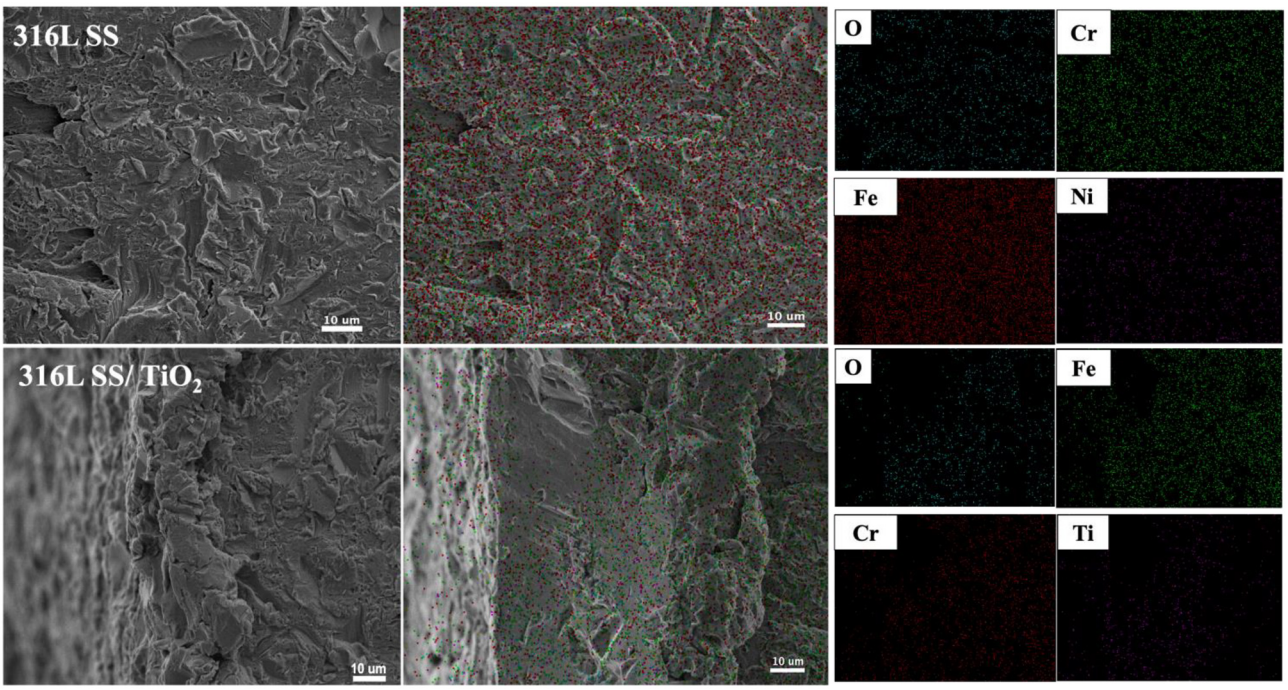

Fig. 1 SEM micrographs of 316L SS and 316L SS/TiO_2 surfaces. SEM micrographs reveal a rough surface because of the sandblasting. In addition to the presence of characteristic elements of SS, mapping analysis confirms the presence of Ti.

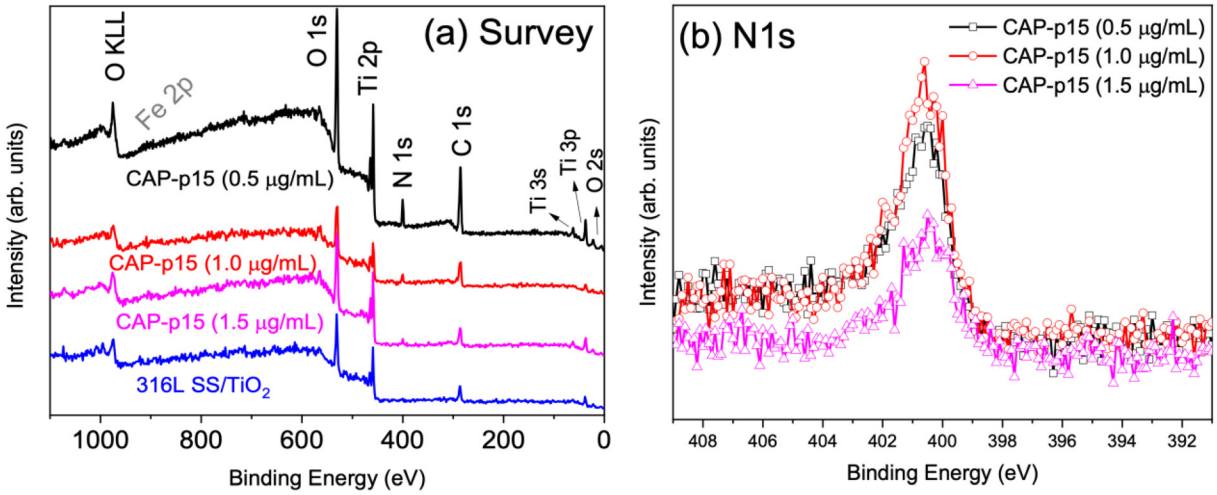

Sample/Composition	C (at. %)	O (at. %)	Ti (at. %)	N (at. %)
316L SS/TiO_2	37.2	49.6	13.2	-
316L SS/TiO_2/CAP-p15 (0.5 μg/mL)	45.2	37.8	11.3	5.7
316L SS/TiO_2/CAP-p15 (1 μg /mL)	49.0	34.8	8.8	7.4
316L SS/TiO_2/CAP-p15 (1.5 μg /mL)	42.4	30.9	21.3	5.4

Fig. 2 The XPS survey spectra of the pristine 316L SS/TiO_2 surface and after functionalization with CAP-p15 peptide at the three concentrations (a). The N content was detected for the 0.5 and 1 μg mL^{-1} samples, while the intensity decreased for the 1.5 μg mL^{-1} sample (b). The table reports the variation in atomic concentrations for all samples.

consistent with a decrease in the intensity of the Ti peaks. However, as shown in Fig. 2a, no variations in the bonding characteristics of the TiO_2 samples are induced by the functionalization process. The three samples presented a single bonding related to Ti having a 4^+ valence state.

Roughness

An optical profilometer was used to analyze the roughness of the 316L SS/TiO_2 pristine and functionalized surfaces with varying peptide concentrations. The images (Fig. 3) reveal that the presence of CAP-p15 at a low concentration (0.5 μg mL^{-1}) leads to a significant reduction in the Sa of 316L SS/TiO_2 surfaces. This is due to the peptide distribution within the grooves and holes of the pristine surface. No statistical differences were found between the 1 μg mL^{-1} and pristine samples. Conversely, the concentration of 1.5 μg mL^{-1} demonstrated a statistically significant increase in Sa, suggesting that higher concentrations facilitate the formation of larger agglomerates on the surface, thereby increasing the average roughness.

Wettability

According to the wettability assay, the 316L SS/TiO_2 surfaces possess a water contact angle measurement of 128.1° after 5 minutes. Functionalized surfaces disclosed a reduction of the contact angles to 22.7° ± 1.69°, 10.6° ± 1.83°, and 3.95° ± 0.7° for concentrations of 0.5, 1 and 1.5 μg mL^{-1}, respectively. This important variation is probably due to the exposure of hydrophilic polar groups from the peptide in contact with water (Fig. 4).

In vitro mineralization

The cumulative release profile of CAP-p15 (Fig. 5) showed an initial burst release of approximately 11% within the first 24 hours, followed by a sustained and gradual release over time. Notably, the 0.5 μg mL^{-1} concentration exhibited a slightly lower cumulative release compared to the 1.0 and 1.5 μg mL^{-1} concentrations. This reduced release can be attributed to the precipitation of mineral phases induced by the incubation in AS, which likely hindered the diffusion of the peptide from the surface.

SEM images (Fig. 6) of the pristine surface reveal the presence of small precipitates, some isolated and others forming aggregates with a size of 20 μm, exhibiting a cauliflower-like morphology with undefined edges. In contrast, functionalized surfaces exhibited deposits with more defined morphologies (spherules) with sizes around 40 μm. The highest concentration of CAP-p15 (1.5 μg mL^{-1}) promoted the formation of a uniform layer with flake-like crystals. The EDX analysis showed a Ca/P ratio of 1.68 for deposits formed on pristine surfaces, while crystals formed with 0.5, 1, and 1.5 μg mL^{-1} peptide concentrations showed Ca/P ratios of 1.9, 1.73, and 1.87, respectively. These values are higher than the stoichiometric value of hydroxyapatite (1.67), indicating possible substitutions in the hydroxyapatite lattice.[30]

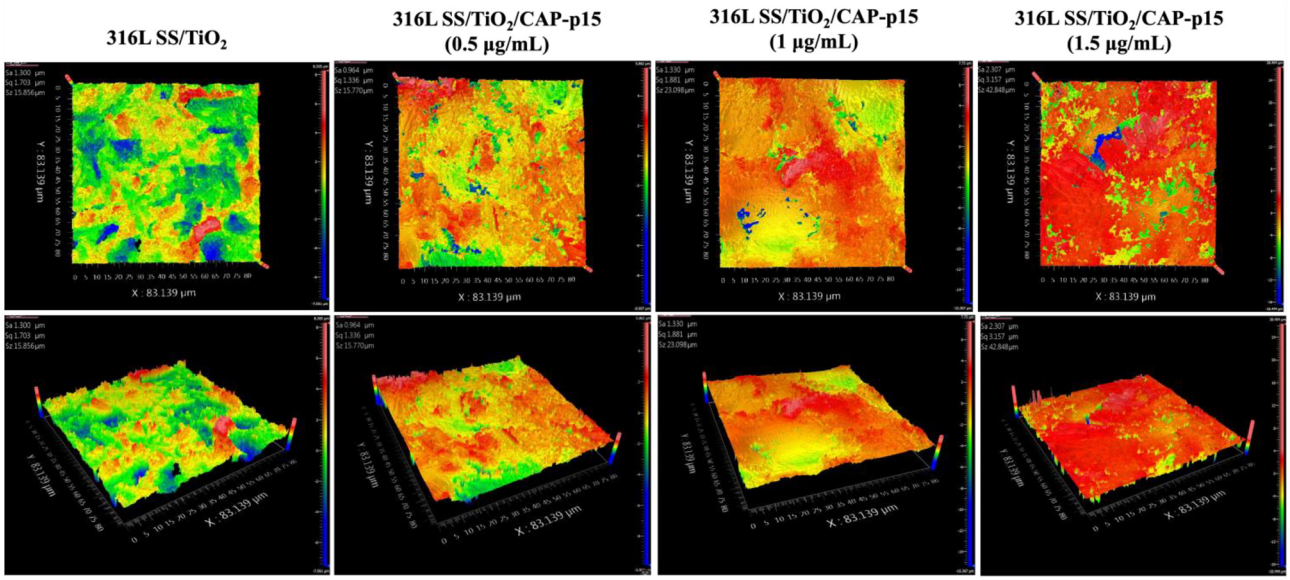

	316LSS/TiO_2	316L SS/TiO_2/ CAP-p15 (0.5 µg/mL)	316L SS/TiO_2/CAP-p15 (1 µg/mL)	316L SS/TiO_2/CAP-p15 (1.5 µg/mL)
Sa (µm)	1.32 ± 0.07	0.87 ±0.06	1.58 ±0.58	2.29 ± 0.29
Max height (µm)	7.81 ± 0.63	5.31 ± 0.48	7.54 ± 0.31	20.28 ± 5.40

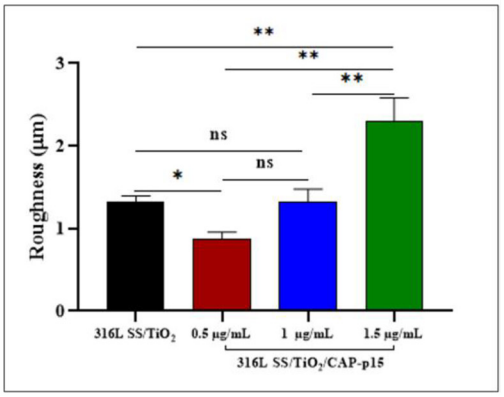

Fig. 3 Roughness analysis. At the lowest concentration, CAP-p15 shows a uniform distribution covering grooves and holes from sandblasting treatment. Additionally, higher concentrations produce larger agglomerates distributed on the surface, reaching heights of 20.28 ± 5.40 µm on surfaces treated with 1.5 µg mL^{-1}. The concentration of 1.5 µg mL^{-1} displayed a higher Sa of 2.29 ± 0.29 µm due to the agglomerates on the surface, no statistical differences between 1 µg mL^{-1} and pristine surfaces. On the other hand, 0.5 µg mL^{-1} of CAP-p15 presented the lowest Sa (0.87 ± 0.06 µm) because of the peptide distribution. One-way ANOVA; ns, no significance; * $p < 0.05$; ** $p < 0.001$.

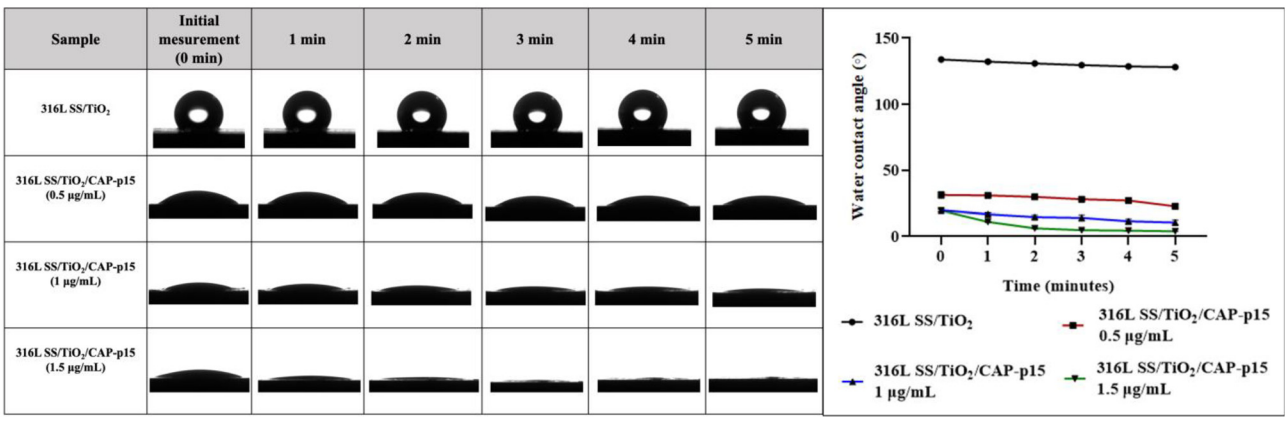

Fig. 4 Contact angle measurement of samples (from 0–5 minutes). The adsorption of CAP-p15 contributes to a decrease in the contact angle as the concentration increases, showing values of 31.25 ± 2.3° to 22.7° ± 1.69° for 0.5 µg mL^{-1}, and 19.85° ± 1.06° to 10.6° ± 1.83°, and 9.55° ± 0.77° to 3.95° ± 0.7° for concentrations of 0.5, 1 and 1.5 µg mL^{-1}, respectively.

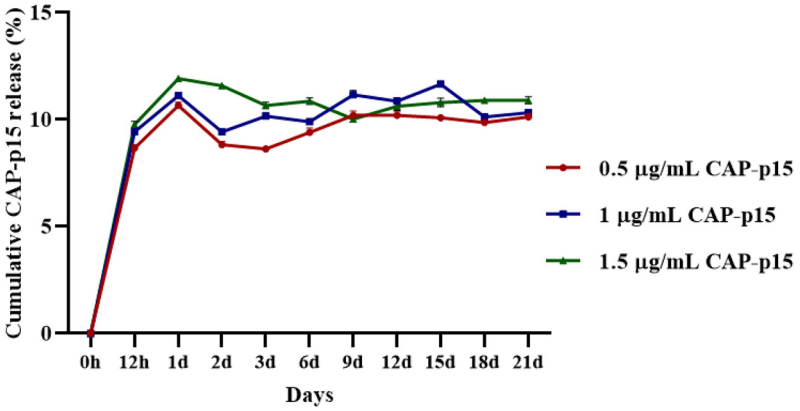

Fig. 5 Cumulative CAP-p15 release of the three concentrations. Data reported as mean ± SD (n = 3).

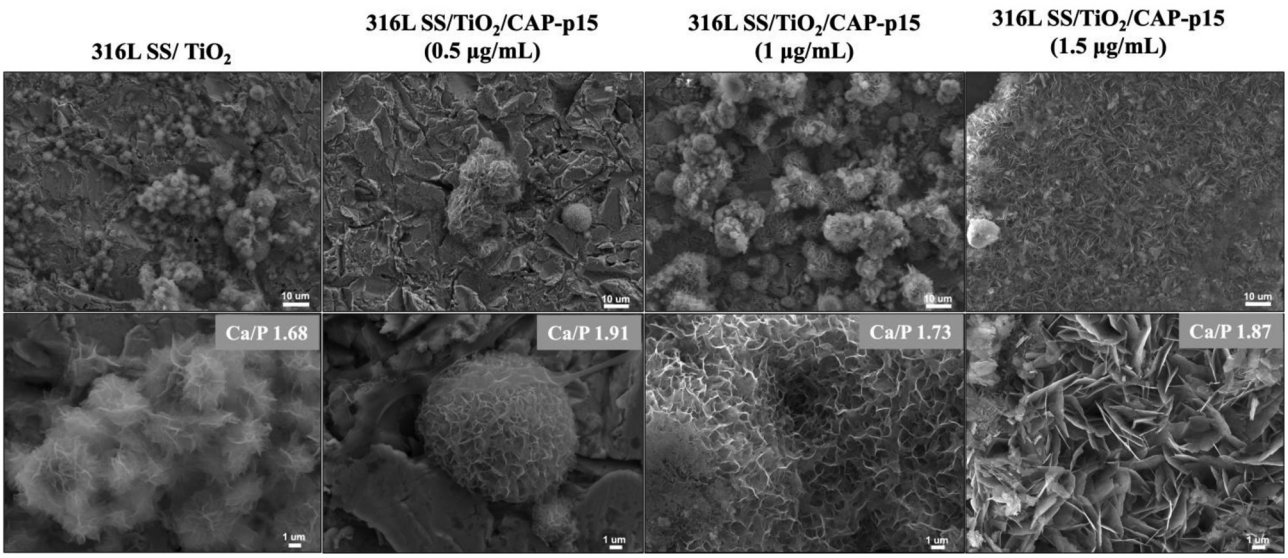

Fig. 6 SEM micrographs obtained after immersion in AS for 21 days display the distribution of small precipitates on the pristine samples with undefined edges. Deposits observed on functionalized surfaces showed spherules and layers formed by flake-like crystals. EDS analysis revealed values of Ca/P close to hydroxyapatite.

Spectroscopy analysis was used to determine the chemical composition of deposits (Fig. 7). ATR spectra of crystals on 316L SS/TiO_2 revealed the presence of bands ν_4 560 cm^{-1}, ν_4 598 cm^{-1}, ν_1 960 cm^{-1}, ν_1 1021 cm^{-1} that corresponds to phosphate groups (PO_4^{3-}), the band at 1645 cm^{-1} corresponds to an OH^- group, and incipient presence of the band ~860 cm^{-1} is characteristic of the adsorbed carbonate group (CO_3^{2-}).[31,32]

These same bands were observed in the deposits formed on functionalized surfaces with CAP-p15, however, the presence of bands corresponding to CO_3^{2-} at ν_2 860 cm^{-1}, ν_1 1318 cm^{-1}, ν_3 1415 cm^{-1}, ν_3 1456 cm^{-1}, and ν_3 1540 cm^{-1}, indicate the presence of predominantly carbonated hydroxyapatite (CHAp) B-type which is the most common substitution in human bones.[30,32] On the other hand, the band around ~1171 cm^{-1} corresponds to ν_3 domain phosphate ions from apatite.[33] Additionally, the discrete band located ~1212 cm^{-1} have been attributed to the HPO_4^{2-} group, specifically in dicalcium phosphate dehydrate (DCPD, brushite).[34] The presence of this band suggests the coexistence of early mineral phases, which is consistent with the dynamic nature of apatite maturation processes.

Cell viability

As shown in Fig. 8, all tested concentrations of CAP-p15 improved the viability of hPDLCs. A noticeable increase in cell viability was observed after 24 hours of culture across all three concentrations evaluated. This improvement was sustained up to 72 hours, particularly at the 0.5 µg mL^{-1} concentration. However, the 1 µg mL^{-1} and 1.5 µg mL^{-1} concentrations also maintained viability percentages above 90%. According to the international standard ISO 10993-5:2009, cell viability below 70% indicates cytotoxicity; therefore, none of the tested concentrations displayed cytotoxic effects.[35]

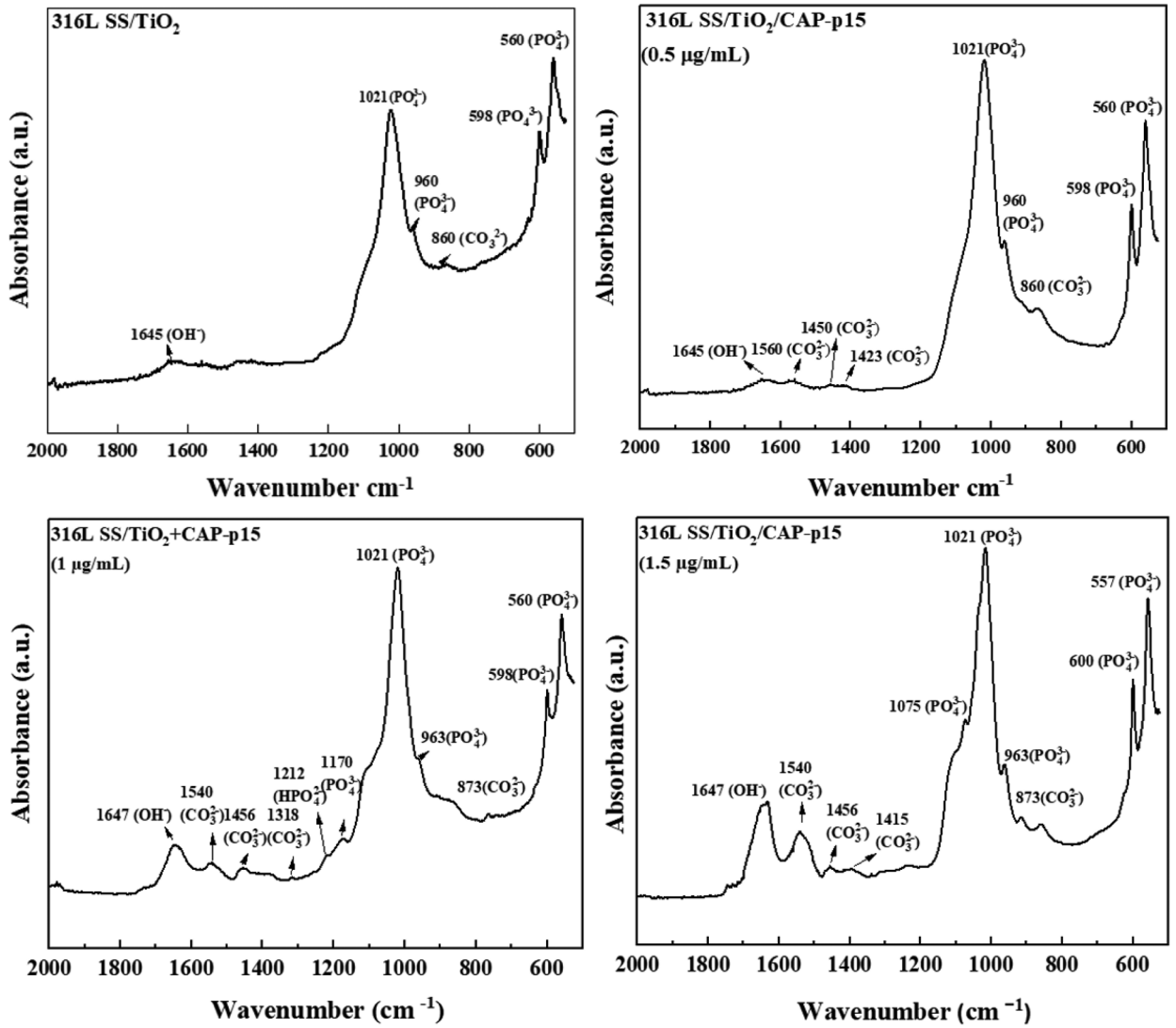

Fig. 7 ATR spectra of precipitation after 21 in AS. All samples display PO_4^{3-} groups corresponding to apatite; however, in functionalized surfaces, it is possible to observe the presence of CO_3^{2-} indicating carbonated hydroxyapatite predominantly B-type.

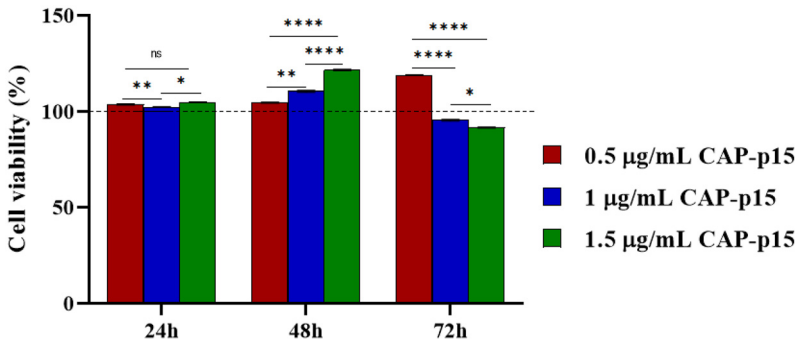

Fig. 8 Percentage of cell viability of hPDLCs cultivated in 316L SS/TiO_2 surfaces treated with CAP-p15 (n = 3). Two-way ANOVA, ns, no significant; * $p < 0.05$, ** $p < 0.001$, **** $p < 0.0001$.

Cell attachment

Fig. 9 illustrates the hPDLC attached to 316L SS/TiO_2 surfaces (43.7%). More importantly, we can see that 316L SS/TiO_2 surfaces functionalized with the three different concentrations CAP-p15 promoted an increase of percentage attached cells after 24 h (140.7%, 93% and 94.1% for 0.5, 1 and 1.5 μg mL^{-1}, respectively). The SEM micrographs reveal that the hPDLC attached on pristine surfaces have a rounded morphology; meanwhile, cells on functionalized samples present cytoplasmic extensions and spread over the surface suggesting a higher viability. Notably, surfaces functionalized with 0.5 μg mL^{-1} concentration of CAP-p15 demonstrated the highest percentage of adhered cells, approximately 3.2-fold higher than the control. These results may indicate that cell attachment could be attributed to the chemical and topographic changes generated by the presence and distribution of CAP-p15 on the 316L SS/TiO_2 surfaces.

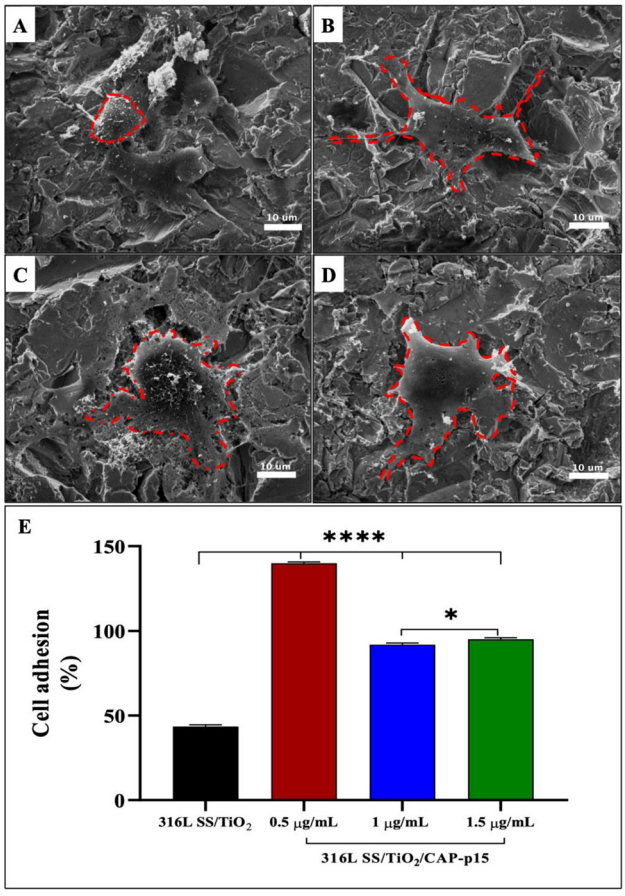

Fig. 9 Morphological analysis (A) reveals that HPDLC attached to pristine surfaces have a rounded morphology. The cell spreads on functionalized surfaces, acquiring polygonal or star-shaped structures (B–D) (highlighted in red). Quantitative analysis of the percentage of HPDLC attached to the substrates (E). All concentrations of CAP-p15 (0.5, 1, and 1.5 μg mL^{-1}) promote an increase (3.2-fold and 2.1-fold) in the percentage of attached cells compared to control surfaces. One-way ANOVA, * $p < 0.05$, **** $p < 0.0001$.

Discussion

Corrosion and inadequate osseointegration remain significant limitations for implants and medical devices made from 316L stainless steel (316L SS). Approximately 20% of SS implants are removed due to corrosion-related complications, including inflammation, allergic reactions, and fibrous encapsulation.[36,37] To address these challenges and improve the interfacial characteristics and long-term performance of SS, several functionalization strategies have been developed. In particular, applying an amorphous TiO_2 coating to rough SS substrates has been shown to enhance osseointegration, promote an anti-inflammatory environment, reduce bacterial attachment, and inhibit biofilm formation, thereby providing an additional layer of protection against infection.[38]

Moreover, incorporating biomolecules such as peptides has emerged as a promising method to provide specific biological cues, thereby enhancing cell attachment and differentiation.[39–41] In this context, our study evaluated the impact of physical adsorption of CAP-p15 peptide at three different concentrations (0.5, 1, and 1.5 μg mL^{-1} of CAP-p15) on 316L SS/TiO_2 substrates. The results indicated a concentration-dependent increase in surface roughness, peaking at 2.2 μm, likely due to weak intermolecular interactions between the negatively charged CAP-p15 and the surface under physiological conditions (37 °C, pH 7.4), as well as peptide self-assembly.

Initially, the pristine 316L SS surface exhibited a high-water contact angle (WCA) of 128°, confirming its hydrophobic nature. After functionalization, WCA progressively decreased by 22.7°, 10.6°, and 3.95° for the 0.5, 1, and 1.5 μg mL^{-1} concentrations of CAP-p15, respectively. This reduction indicates a shift toward a more hydrophilic surface, and the effect appears to be dependent on peptide concentration. It is well established that surfaces with WCA values below 90° are considered hydrophilic, whereas values above 90° indicate hydrophobicity.[42] Previous studies have indicated that nanoscale and microscale surface roughness, along with hydrophilic properties, can enhance early cellular responses such as adhesion and differentiation compared to hydrophobic surfaces.[43]

Notably, CAP-p15 adsorption onto amorphous TiO_2 surfaces has been reported to promote the formation of nanospherical structures, further increasing the surface roughness.[21] Roughness is a key parameter in implant osseointegration, influencing initial cell–surface interactions such as adhesion and proliferation. Although there is no universal optimal roughness value, several studies suggest that moderate Sa values (~1–2 μm) can enhance the bone implant contact (BIC) more effectively than either smoother surfaces or those with Sa values exceeding 2 μm.[10,44]

Interestingly, the 0.5 μg mL^{-1} concentration resulted in the lowest surface roughness, due to a more homogeneous distribution of the peptide across the surface grooves. This homogeneity may expose more active peptide sites, facilitating cellular interaction despite the lower roughness. In contrast, higher concentrations (1 and 1.5 μg mL^{-1}) resulted in the for-

mation of larger peptide aggregates (Fig. 3), which can be attributed to the intrinsic hydrophobicity of CAP-p15.

Numerous studies have been conducted to enhance the surface properties of SS through topographical or chemical modifications.[45–47] For instance, Majhi *et al.*[45] reported that the peptide KLLLLRLRKLLLRR (KLR) on SS substrates promoted an increase in roughness while contributing to a decrease in the contact angle, decreasing it to slightly below 90°. This slight tendency toward hydrophobicity was attributed to the presence of alkyl groups in APTES molecules, which are necessary for covalent binding. In contrast, our results demonstrate that the physical binding of CAP-p15 promotes a decrease in hydrophobicity, resulting in contact angles within the hydrophilic range.

To demonstrate the ability of CAP-p15 to induce mineral formation, we incubate the samples in AS for 21 days. During this period, the cumulative peptide release of the three concentrations of CAP-p15 were measured. A slightly lower release was observed for the concentration 0.5 μg mL^{-1} compared to higher concentrations. Additionally, the reduction in release can be attributed to the precipitation of mineral phases induced by incubation in AS, which likely hindered the diffusion of the peptide from the material surface. After the incubation period, all surfaces functionalized with CAP-p15 showed the formation of deposits with flake-like crystals of varying sizes, dependent on the peptide concentration; in contrast, pristine surfaces exhibited cauliflower-like crystals with undefined edges. The spectroscopic analysis of precipitates showed the presence of phosphate groups characteristic of apatite. However, at concentrations of 1 and 1.5 μg mL^{-1}, we also observed carbonate groups characteristic of carbonated hydroxyapatite, which is present in physiological mineralized tissue. The nucleation of these precipitates is related to the distribution of CAP-p15 on 316L SS/TiO_2 surfaces, which act as templates for the nucleation of calcium phosphates, as observed in proteins such as amelogenin and peptides derived from it.[48] *In silico* analysis demonstrates that CAP-p15 has an isoelectric point of 5.48, indicating a negative charge at physiological pH allowing it to interact with calcium ions and thereby facilitate mineral nucleation.[21]

Finally, the biocompatibility was assessed through a cell viability assay, the results display values above 90% after 72 hours of cell culture, confirming the absence of cytotoxic effects. This aligns finding by Ureiro-Cueto *et al.*[13] where the adsorption of CAP-p15 enhanced the cell proliferation and even the differentiation of mesenchymal stem cells. Cell attachment was evaluated after 24, the SEM analysis showed that hPDLC cells on the functionalized surfaces exhibited a cuboidal morphology with numerous cytoplasmic extensions, indicating strong cell–surface interactions. These observations are consistent with other studies where SS surfaces were functionalized with peptides such as RGD, REDV, and KLR, contributed to increased cell attachment, and even showed antibacterial properties; however, covalent peptide immobilization still presents challenges, particularly related to the use of linkers.[39,40,45]

Despite the inherent limitations of physical adsorption (*e.g.* uncontrolled peptide release and activity loss), our results reveal the potential of CAP-p15 as a bioactive molecule for developing new surface functionalization strategies for bone tissue regeneration.

Conclusions

The physical adsorption of CAP-p15 onto 316L SS/TiO_2 surfaces, induced changes in surface chemistry, roughness and wettability promoting the formation of carbonated apatite. Notably, a lower concentration of CAP-p15 significantly enhanced cell viability and attachment compared to the 1 and 1.5 μg mL^{-1} concentrations. These findings suggest that CAP-p15 biopeptide possesses potential applications in bone tissue regeneration for stainless steel implants.

Author contributions

G. U. C, G. M. A and S. E. R, conceptualization; G. U. C and S. E. R, methodology; G. U. C and G. M. A, data analysis; G. U. C, writing; G. M. A, S. E. R and H. A, paper review and editing, H. A, G. M. A and S. E. R, supervision; L. H. R and J. O. F. F, validation.

Conflicts of interest

The authors confirm that there are no known conflicts of interest associated with this publication and there has been no financial support that could have influenced our outcomes.

Data availability

This work is part of MX Patent No. 348746, for which the data cannot be made available due to legal or ethical confidentiality requirements.

Acknowledgements

Guadalupe Ureiro-Cueto acknowledges e Programa de Maestría y Doctorado en Ciencias Médicas, Odontológicas y de la Salud (PMDCMOS-UNAM) and Secretaria de Ciencia, Humanidades, Tecnología e Innovación (SECIHTI) for a fellowship.

The authors thank to Dr Selene Rubí Islas Sánchez from the Institute of Applied Sciences and Technology (ICAT_LUCE, UNAM) for supporting spectroscopic techniques; Biol. Armando Zepeda and Francisco Pasos, from the Laboratory of Morphology and Toxicology of the Department of Cell and Tissue Biology, Faculty of Medicine, UNAM, for their technical assistance in SEM imaging; Phys. Lázaro Huerta Arcos from IIM, UNAM, for the technical assistant in the XPS analysis.

The authors are grateful for financial support from DGAPA-PAPIIT grant numbers IT200123 and IN206723. This work is part of the MX Patent No. 348746.

References

1 A. Bekmurzayeva, W. J. Duncanson, H. S. Azevedo and D. Kanayeva, Surface Modification of Stainless Steel for Biomedical Applications: Revisiting a Century-old Material, *Mater. Sci. Eng., C*, 2018, **93**, 1073–1089.

2 S. Ali, M. Irfan, U. M. Niazi, A. M. A. Rani, A. Rashedi, S. Rahman, *et al.*, Microstructure and Mechanical Properties of Modified 316L Stainless Steel Alloy for Biomedical Applications Using Powder Metallurgy, *Materials*, 2022, **15**(8), 2822.

3 G. Mani, D. Porter, S. Collins, T. Schatz, A. Ornberg and R. Shulfer, A Review on Manufacturing Processes of Cobalt–Chromium Alloy Implants and Its Impact on Corrosion Resistance and Biocompatibility, *J. Biomed. Mater. Res., Part B*, 2024, **112**(6), e35431.

4 E. W. F. Sabará, V. Pereira, A. L. Molisani, L. Caldeira, R. C. Souza, T. A. Simões, *et al.*, Electrochemical Behaviour and Microstructural Characterization of Different Austenitic Stainless Steel for Biomedical Applications, *Mater. Res. Express*, 2020, **7**(10), 105402.

5 D. Święch, G. Palumbo, N. Piergies, E. Pięta, A. Szkudlarek and C. Paluszkiewicz, Spectroscopic Investigations of 316L Stainless Steel under Simulated Inflammatory Conditions for Implant Applications: The Effect of Tryptophan as Corrosion Inhibitor/Hydrophobicity Marker, *Coatings*, 2021, **11**(9), 1097.

6 N. Sultana, Y. Nishina and M. Z. I. Nizami, Surface Modifications of Medical Grade Stainless Steel, *Coatings*, 2024, **14**(3), 248.

7 Y. K. Erdogan and B. Ercan, Anodized Nanostructured 316L Stainless Steel Enhances Osteoblast Functions and Exhibits Anti-Fouling Properties, *ACS Biomater. Sci. Eng.*, 2023, **9**(2), 693–704.

8 S. A. Gehrke, J. H. Cavalcanti de Lima, F. Rodriguez, J. L. Calvo-Guirado, J. Aramburú Júnior, L. Pérez-Díaz, *et al.*, Microgrooves and Microrugosities in Titanium Implant Surfaces: An In Vitro and In Vivo Evaluation, *Materials*, 2019, **12**(8), 1287.

9 W. He, P. Yao, D. Chu, H. Sun, Q. Lai, Q. Wang, *et al.*, Controllable Hydrophilic Titanium Surface with Micro-protrusion or Micro-groove Processed by Femtosecond Laser Direct Writing, *Opt. Laser Technol.*, 2022, 108082.

10 T. Albrektsson and A. Wennerberg, Oral implant surfaces: Part 1–Review Focusing on Topographic and Chemical Properties of Different Surfaces and In Vivo Responses to them, *Int. J. Prosthodont.*, 2004, **17**(5), 536–543.

11 W. Y. Choi, J. K. Lee, D. S. Choi and I. Jang, Improved Osseointegration of Dental Titanium Implants by TiO_2 Nanotube Arrays with Recombinant Human Bone Morphogenetic Protein-2: A Pilot In Vivo Study, *Int. J. Nanomed.*, 2015, **1145**, 1145–1154.

12 H. Zheng, L. Xu, Y. Jiao, Y. Xia, X. Wu, K. Lu, *et al.*, Fabrication and Surface Characterization of Titanium Dioxide Nanotubes on Titanium Implants, *Front. Mater.*, 2023, **10**, 1–8.

13 G. Ureiro-Cueto, S. E. Rodil, P. Silva-Bermúdez, M. Santana-Vázquez, L. Hoz-Rodríguez, H. Arzate, *et al.*, Amorphous Titanium Oxide ($aTiO_2$) Thin Films Biofunctionalized with CAP-p15 Induce Mineralized-like Differentiation of Human Oral Mucosal Stem Cells (hOMSCs), *Biomed. Mater.*, 2024, **19**(5), 055003.

14 S. Makihira, T. Shuto, H. Nikawa, K. Okamoto, Y. Mine, Y. Takamoto, *et al.*, Titanium Immobilized with an Antimicrobial Peptide Derived from Histatin Accelerates the Differentiation of Osteoblastic Cell Line, MC3T3-E1, *Int. J. Mol. Sci.*, 2010, **11**(4), 1458–1470.

15 P. Kämmerer, M. Heller, J. Brieger, M. Klein, B. Al-Nawas and M. Gabriel, Immobilisation of Linear and Cyclic RGD-peptides on Titanium Surfaces and their Impact on Endothelial Cell Adhesion and Proliferation, *Eur. Cells Mater.*, 2011, **21**, 364–372.

16 B. Nie, H. Ao, J. Zhou, T. Tang and B. Yue, Biofunctionalization of Titanium with Bacitracin Immobilization Shows Potential for Anti-bacteria, Osteogenesis and Reduction of Macrophage Inflammation, *Colloids Surf., B*, 2016, **145**, 728–739.

17 L. D. Trino, E. S. Bronze-Uhle, A. Ramachandran, P. N. Lisboa-Filho, M. T. Mathew and A. George, Titanium Surface Bio-functionalization Using Osteogenic Peptides: Surface Chemistry, Biocompatibility, Corrosion and Tribocorrosion Aspects, *J. Mech. Behav. Biomed. Mater.*, 2018, **81**, 26–38.

18 S. S. Hakki, S. B. Bozkurt, E. Türkay, M. Dard, N. Purali and W. Götz, Recombinant Amelogenin Regulates the Bioactivity of Mouse Cementoblasts In Vitro, *Int. J. Oral Sci.*, 2018, **10**(2), 15.

19 S. Han, X. Peng, L. Ding, J. Lu, Z. Liu, K. Wang, *et al.*, TVH-19, a Synthetic Peptide, Induces Mineralization of Dental Pulp Cells In Vitro and Formation of Tertiary Dentin In Vivo, *Biochem. Biophys. Res. Commun.*, 2021, **534**, 837–842.

20 M. Fan, Z. Zhou, W. Zhu, M. Li, Y. Tu, Z. Yu, *et al.*, Reinforced Dentin Remineralization Via a Novel Dual-affinity Peptide, *Dent. Mater.*, 2024, **40**(2), 254–266.

21 G. Ureiro-Cueto, S. E. Rodil, M. Santana-Vázquez, L. Hoz-Rodriguez, H. Arzate and G. Montoya-Ayala, Characterization of $aTiO_2$ Surfaces Functionalized with CAP–p15 Peptide, *J. Biomed. Mater. Res., Part A*, 2024, 1399–1411.

22 S. E. Rodil, C. Ramírez, R. Olivares, H. Arzate, J. Réyes-Gasga and C. Magaña, Osteoblasts Attachment on Amorphous Carbon Films, *Diamond Relat. Mater.*, 2006, **15**(9), 1300–1309.

23 G. Ramírez, S. E. Rodil, H. Arzate, S. Muhl and J. J. Olaya, Niobium Based Coatings for Dental Implants, *Appl. Surf. Sci.*, 2011, **257**(7), 2555–2559.

24 P. Silva–Bermudez, A. Almaguer–Flores, V. I. Garcia, R. Olivares–Navarrete and S. E. Rodil, Enhancing the

Osteoblastic Differentiation Through Nanoscale Surface Modifications, *J. Biomed. Mater. Res., Part A*, 2017, **105**(2), 498–509.

25 M. Fernández-Lizárraga, J. García-López, S. E. Rodil, R. M. Ribas-Aparicio and P. Silva-Bermudez, Evaluation of the Biocompatibility and Osteogenic Properties of Metal Oxide Coatings Applied by Magnetron Sputtering as Potential Biofunctional Surface Modifications for Orthopedic Implants, *Materials*, 2022, **15**(15), 5240.

26 Q. Ruan, N. Siddiqah, X. Li, S. Nutt and J. Moradian-Oldak, Amelogenin–chitosan Matrix for Human Enamel Regrowth: Effects of Viscosity and Supersaturation Degree, *Connect. Tissue Res.*, 2014, **55**(sup1), 150–154.

27 Q. Ruan, Y. Zhang, X. Yang, S. Nutt and J. Moradian-Oldak, An amelogenin–chitosan Matrix Promotes Assembly of an Enamel-like Layer with a Dense Interface, *Acta Biomater.*, 2013, **9**(7), 7289–7297.

28 S. Prajapati, Q. Ruan, K. Mukherjee, S. Nutt and J. Moradian-Oldak, The Presence of MMP-20 Reinforces Biomimetic Enamel Regrowth, *J. Dent. Res.*, 2018, **97**(1), 84–90.

29 E. G. Hayman, E. Engvall, E. A'Hearn, D. Barnes, M. Pierschbacher and E. Ruoslahti, Cell Attachment on Replicas of SDS Polyacrylamide Gels Reveals Two Adhesive Plasma Proteins, *J. Cell Biol.*, 1982, **95**(1), 20–23.

30 L. Russo, F. Taraballi, C. Lupo, A. Poveda, J. Jiménez-Barbero, M. Sandri, *et al.*, Carbonate Hydroxyapatite Functionalization: A Comparative Study Towards (Bio)molecules Fixation, *Interface Focus*, 2014, **4**(1), 20130040.

31 J. P. Lafon, E. Champion and D. Bernache-Assollant, Processing of AB-type Carbonated Hydroxyapatite $Ca10_{-x}(PO_4)_{6-x}(CO_3)_x(OH)_{2-x-2y}(CO_3)_y$ Ceramics with Controlled Composition, *J. Eur. Ceram. Soc.*, 2008, **28**(1), 139–147.

32 A. Sroka-Bartnicka, L. Borkowski, G. Ginalska, A. Ślósarczyk and S. G. Kazarian, Structural Transformation of Synthetic Hydroxyapatite Under Simulated In Vivo Conditions Studied with ATR-FTIR Spectroscopic Imaging, *Spectrochim. Acta, Part A*, 2017, **171**, 155–161.

33 C. Rey, M. Shimizu, B. Collins and M. J. Glimcher, Resolution-enhanced Fourier Transform Infrared Spectroscopy Study of the Environment of Phosphate Ion in the Early Deposits of a Solid Phase of Calcium Phosphate in Bone and Enamel and their Evolution with Age: 2. Investigations in the 3 PO_4 Domain, *Calcif. Tissue Int.*, 1991, **49**(6), 383–388.

34 I. V. Smirnov, J. V. Rau, M. Fosca, A. De Bonis, A. Latini, R. Teghil, *et al.*, Structural Modification of Titanium Surface by Cctacalcium Phosphate via Pulsed Laser Deposition and Chemical Treatment, *Bioact. Mater.*, 2017, **2**(2), 101–107.

35 F. Burkhardt, B. C. Spies, C. Wesemann, C. G. Schirmeister, E. H. Licht, F. Beuer, *et al.*, Cytotoxicity of Polymers Intended for the Extrusion-based Additive Manufacturing of Surgical Guides, *Sci. Rep.*, 2022, **12**(1), 7391.

36 E. K. Brooks, R. P. Brooks and M. T. Ehrensberger, Effects of Simulated Inflammation on the Corrosion of 316L Stainless Steel, *Mater. Sci. Eng., C*, 2017, **71**, 200–205.

37 M. J. K. Lodhi, K. M. Deen, M. C. Greenlee-Wacker and W. Haider, Additively Manufactured 316L Stainless Steel with Improved Corrosion Resistance and Biological Response for Biomedical Applications, *Addit. Manuf.*, 2019, **27**, 8–19.

38 V. I. Garcia-Perez, K. M. Hotchkiss, P. Silva-Bermudez, M. M. Hernández, G. Prado-Prone, R. Olivares-Navarrete, *et al.*, Amorphous TiO_2 Nano-coating on Stainless Steel to Improve its Biological Response, *Biomed. Mater.*, 2024, **19**(5), 055037.

39 G. R. Alas, R. Agarwal, D. M. Collard and A. J. García, Peptide-functionalized Poly [oligo(ethylene glycol) methacrylate] Brushes on Dopamine-coated Stainless Steel for Controlled Cell Adhesion, *Acta Biomater.*, 2017, **59**, 108–116.

40 X. Xu, L. Wang, G. Wang and Y. Jin, The Effect of REDV/TiO_2 Coating Coronary Stents on In-stent Restenosis and Re-endothelialization, *J. Biomater. Appl.*, 2017, **31**(6), 911–922.

41 L. Apitius, S. Buschmann, C. Bergs, D. Schönauer, F. Jakob, A. Pich, *et al.*, Biadhesive Peptides for Assembling Stainless Steel and Compound Loaded Micro–Containers, *Macromol. Biosci.*, 2019, **19**(9), e1900125.

42 R. A. Gittens, L. Scheideler, F. Rupp, S. L. Hyzy, J. Geis-Gerstorfer, Z. Schwartz, *et al.*, A Review on the Wettability of Dental Implant Surfaces II: Biological and Clinical Aspects, *Acta Biomater.*, 2014, **10**(7), 2907–2918.

43 C. Eriksson, H. Nygren and K. Ohlson, Implantation of Hydrophilic and Hydrophobic Titanium Discs in Rat TIbia: Cellular Reactions on the Surfaces During the First 3 Weeks in Bone, *Biomaterials*, 2004, **25**(19), 4759–4766.

44 G. A. F. Silva, F. Faot, W. J. da Silva and A. A. Del Bel Cury, Does Implant Surface Hydrophilicity Influence the Maintenance of Surface Integrity After Insertion into Low-density Artificial Bone?, *Dent. Mater.*, 2021, **37**(2), e69–e84.

45 S. Majhi, V. C. Peddiraju and A. Mishra, Effect of Antimicrobial Peptide (AMP)–tethered Stainless Steel Surfaces on the Bacterial Membrane, *Mater. Today Chem.*, 2021, **21**, 100541.

46 K. Piotrowska, M. Madej and D. Ozimina, Assessment of the Functional Properties of 316L Steel Alloy Subjected to Ion Implantation Used in Biotribological Systems, *Materials*, 2021, **14**(19), 5525.

47 V. K. S. Hsiao, Y. C. Lin, H. C. Wu and T. I. Wu, Surface Morphology and Human MG-63 Osteoblasic Cell Line Response of 316L Stainless Steel after Various Surface Treatments, *Metals*, 2023, **13**(10), 1739.

48 S. Habelitz, P. K. DenBesten, S. J. Marshall, G. W. Marshall and W. Li, Self–assembly and Effect on Crystal Growth of the Leucine–rich Amelogenin Peptide, *Eur. J. Oral Sci.*, 2006, **114**(s1), 315–319.